Electronic Supplementary Material (ESI) for Nanoscale.
This journal is © The Royal Society of Chemistry 2014

Supporting Information

Bio-inspired inner-motile photocatalyst film: a magnetically actuated artificial cilia photocatalyst

Dunpu Zhang, Wei Wang, Fengping Peng, Jiahui Kou, Yaru Ni, Chunhua Lu*, Zhongzi Xu*

State Key Laboratory of Materials-Orient Chemical Engineering, College of Materials Science and Engineering, Nanjing University of Technology, Nanjing 210009, People's Republic of China.

Fax: +86 25 83587220, Tel.: +86 25 83587252,

E-mail: chhlu@njtech.edu.cn; zzxu@njtech.edu.cn.

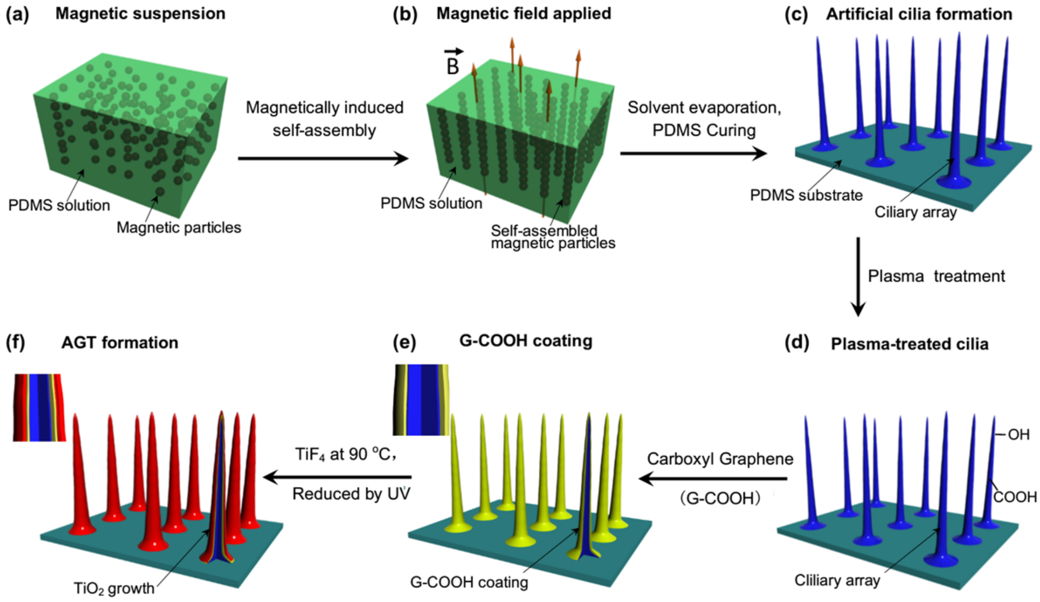

Fig. S1 The fabrication scheme of the AGT. a-c, Preparation of magnetically actuated artificial cilia by magnetic-field-induced self-assembly of magnetic particles method with PDMS matrix. d, The array was treated with plasma treatment. e, Preparation of G-COOH coated arrays (ciliary array@G–COOH, AG). f, Grown TiO_2 on the surface of AG and reduction of G–COOH by UV irradiation (ciliary array@rG–COOH@TiO_2, AGT).

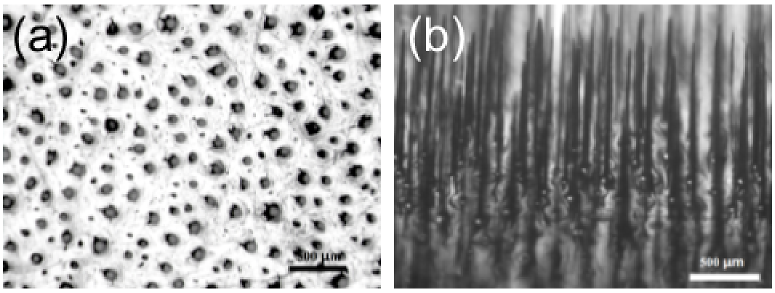

Fig. S2 Optical microscope of the artificial cilia with 1 mm in height. a, Top-view microscope image shows the random spot patterns of the ciliary array. b, Cross-sectional stereoscopic microscope image shows the uniform and vertically aligned ciliary arrays on the surface.

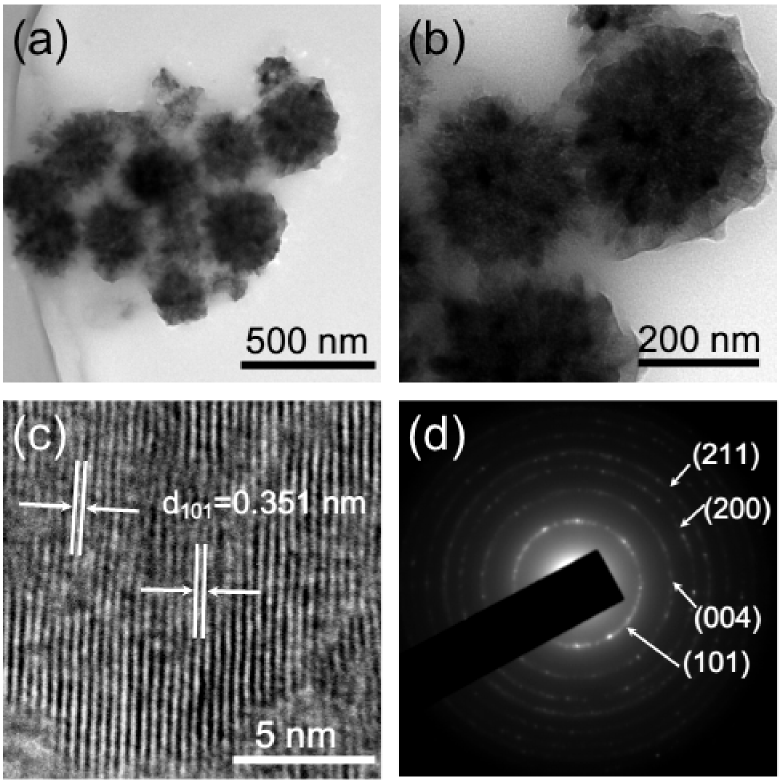

Fig. S3 TEM images of rG–COOH/TiO_2 obtained from AGT. a,b, low and high-magnification images. c, high-resolution TEM image (HRTEM). d, selected area electron diffraction pattern of the TiO_2 nanoclusters. TEM were measured on JEM-200CX.

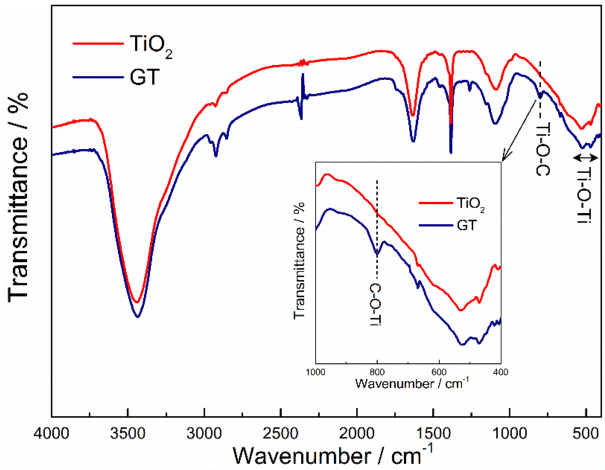

Fig. S4 FTIR spectra of TiO_2 and rG–COOH@TiO_2 (GT) powder. The TiO_2 powder was collected from the growth solution of AGT array, and the rG–COOH@TiO_2 (GT) powder was carefully peeled from the AGT array with the aid of microscope. Fourier transform infrared (FTIR) spectra were measured with a Nexus 670 infrared spectrophotometer. The appearance of a peak located at 800 cm^{-1} is attributed to C–O–Ti vibration in the FTIR spectrum of GT.

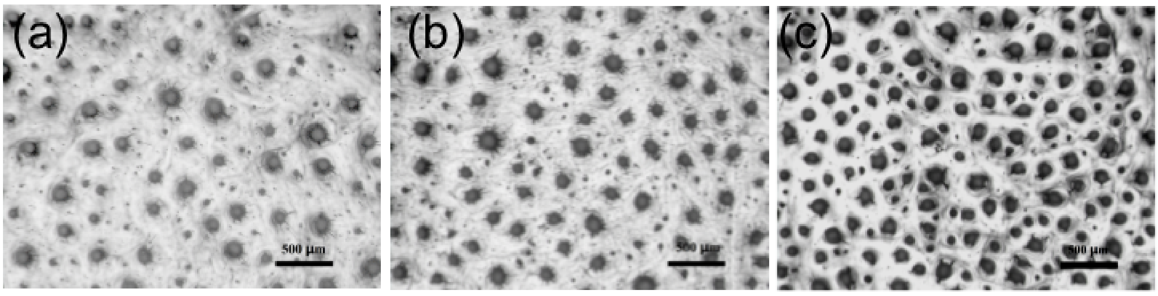

Fig. S5 Array density with tunable Co concentration for 3 mm array. a, Co concentration of 0.9 wt.%, A09. b, Co concentration of 1.2 wt.%, A12. c, Co concentration of 1.5 wt.%, A15. The number density of the array is 890, 1140 and 2310 cm^{-2} for A09, A12 and A15, respectively.

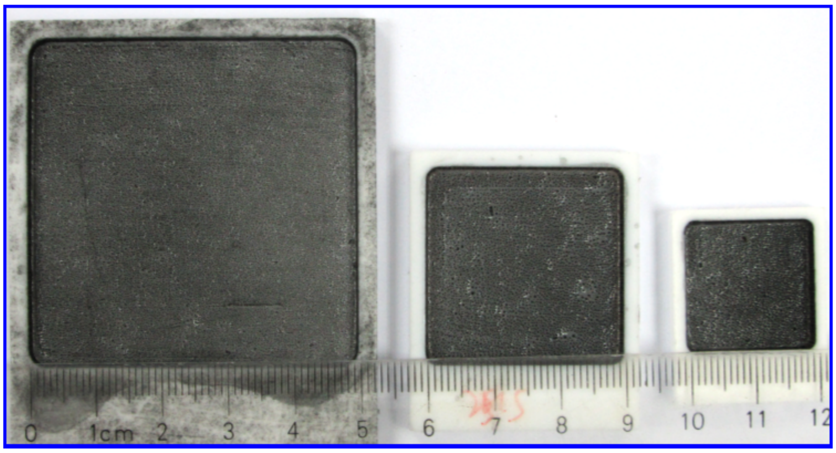

Fig. S6 Digital images of the artificial cilia with various dimensions in the mold. The dimension of array can be as large as 50 mm× 50 mm. As indicated in the digital images, the obtained artificial cilia shows highly uniform and homogeneous characterization.

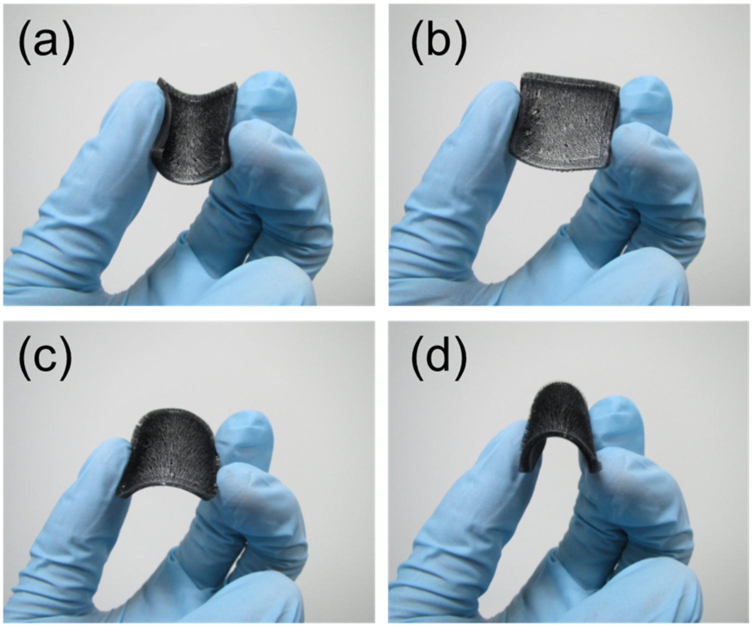

Fig. S7 The high mechanical stability and structural flexibility of the artificial cilia. The artificial cilia is self-supporting, yet can be bended to any specific angle and shape.

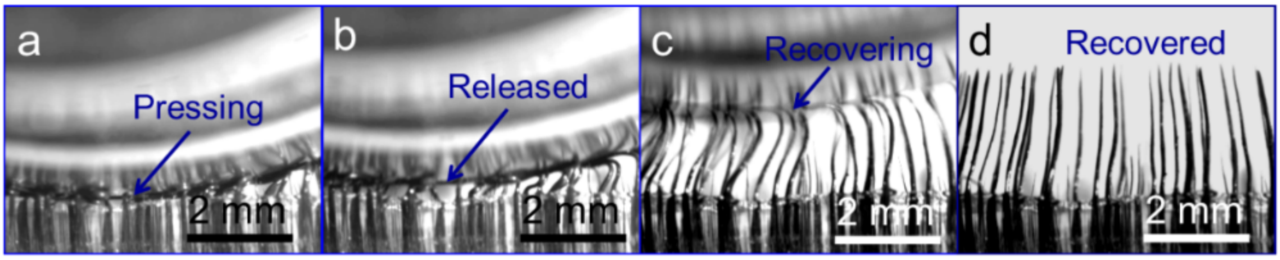

Fig. S8 Structural stability and flexibility of the artificial cilia. The obtained self-supporting AGT possess highly mechanical stability and structural flexibility. They can recover to the original state even experienced mechanical destroy, such as press or wrinkle, with or without magnetically induced. These characterizations make them an ideal candidate for working in more destructive conditions, benefiting from their respondence to the non-contact magnetic field.

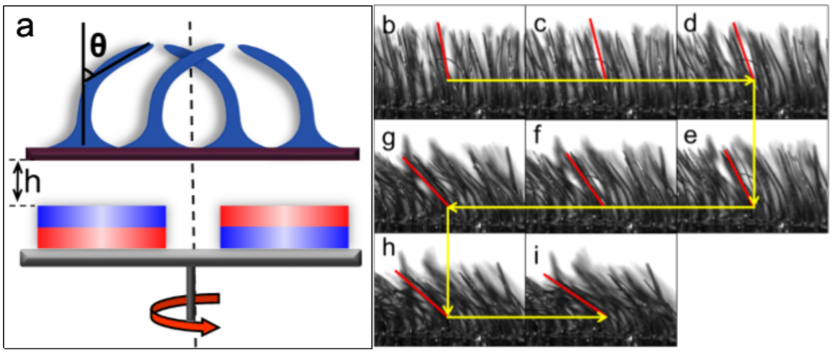

Fig. S9 Tilt angle of the AGT under magnetic actuation. a, Schematic illustration of bending angle of the AGT induced by a pair of magnets. The tilt angle θ is determined by the perpendicular position h of the magnets relative to the sample. b-i, Optical micrographs of bended AGT with varied distance h. The distance h was varied: b, 35 mm. c, 30.0 mm. d, 25.0 mm. e, 20.0 mm. f, 17.5 mm. g, 15.0 mm. h, 12.5 mm. i, 10.0 mm.

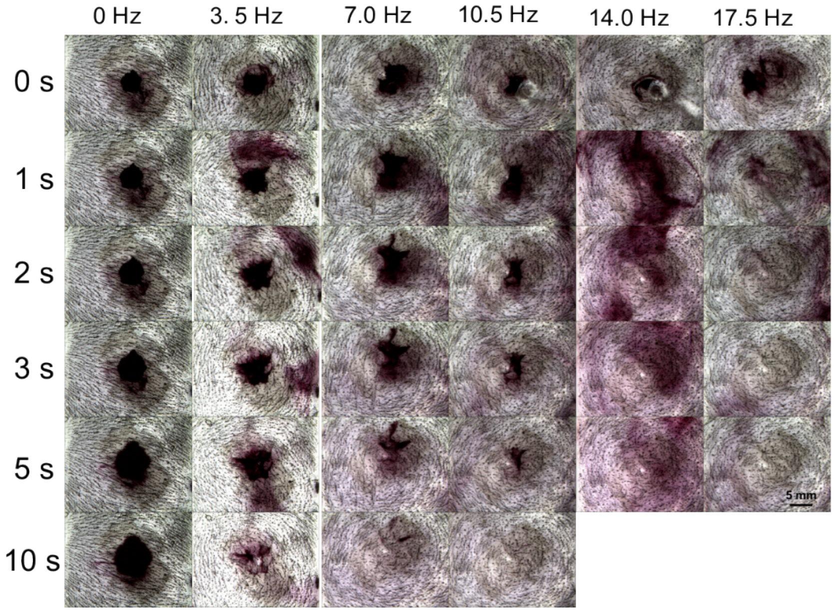

Fig. S10 Time-lapse flow mixing behaviors of the AGT under actuated at various frequencies compared with diffusive mixing. In the experiment, 5 μL red color aqueous was used for all the case. As indicated by the optical images, the mixing could be well done by the AGT *in site* without depending on other external methods. The mixing performance could be controlled by magnetically-actuated frequency. When actuated at 14.0 and 17.5 Hz, the AGT array could give very fast mass transfer due to the violent flow fluctuations caused by mimicking the ciliary motion.

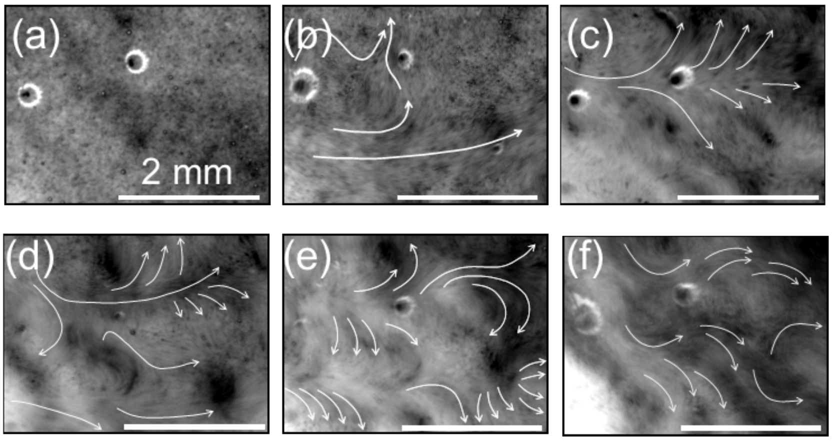

Fig. S11 The net fluidic vortex pattens and distributions caused by the actuated AGT as the function of frequency. a, 0 Hz, b, 3.5 Hz, c, 7.0 Hz, d, 10.5 Hz, e, 14.0 Hz, and f, 17.5 Hz. The scale bar is 2 mm. The cilia-driven vorticies around the actuated AGT can be clearly seen in the optical visualisation, and indicate that the induced flow vortex is much greater when actuated at higher frequency.

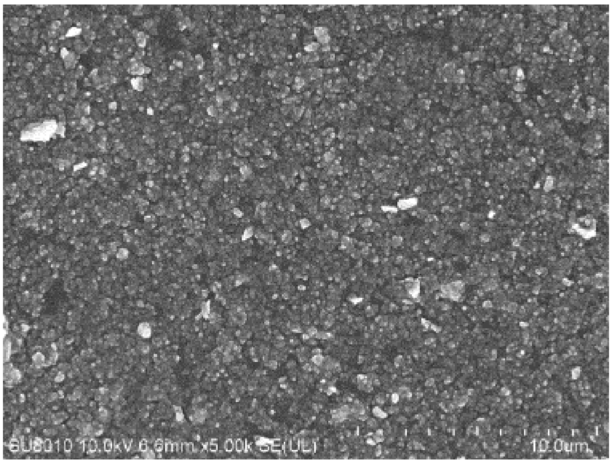

Fig. S12 FESEM image of PGT (planar@rG–COOH@TiO_2). TiO_2 was grown on the surface of planar PDMS sheet by the same experimental method of AGT array as a reference photocatalyst film.

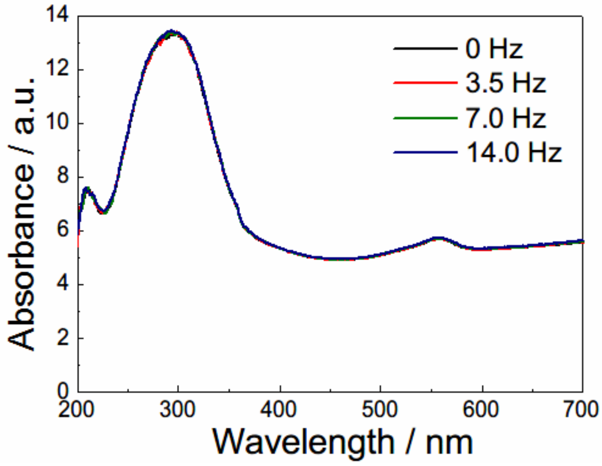

Fig. S13 Optical absorption performance for 3 mm AGT sample with tilt angle of 55 ° (10 mm) at various actuated frequency, indicating that actuated frequency shows negligible effect on the absorption behavior of the AGT.

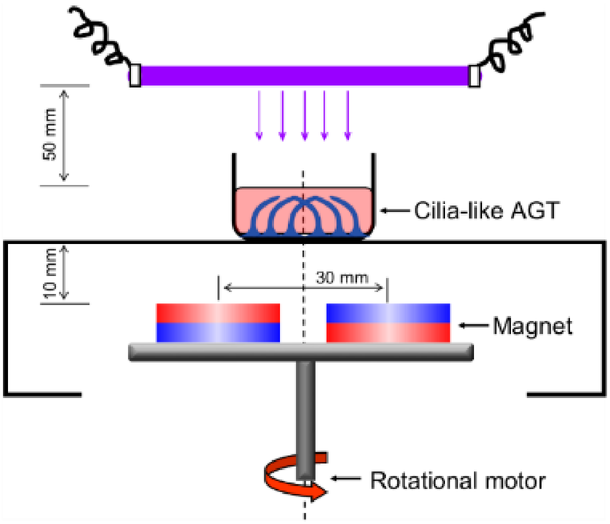

Fig. S14 Schematic drawing of experimental setup for photocatalytic test with 3 mm in height AGT under magnetic actuation. The actuated magnetic field was provided by a pair of flat permanent circular magnets (Neodymium, N52, 25 mm in diameter and 5 mm in thickness), which were symmetrically placed on the rotational motor with distance of 30 mm. The paired permanent magnet were placed 10 mm below the sample with their surface parallel to the substrate and perpendicular to the array direction. The distance between UV lamp and the AGT sample is 50 mm.

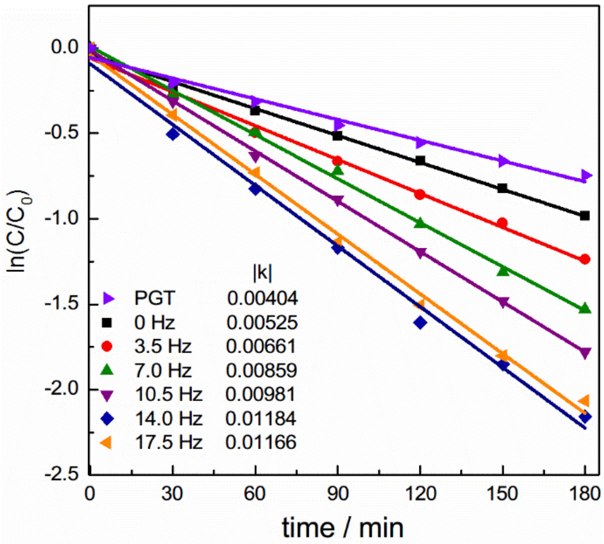

Fig. S15 Photocatalytic kinetics curves of AGT at various magnetically-actuated frequency. The kinetics could be quantitatively evaluated by the Langmuir-Hinshelwood first-order model as following:

$$\ln(\frac{C}{C_0}) = -k\,\mathrm{t} \tag{1}$$

where k is the apparent reaction rate constants (min^{-1}). This model is generally used for the photocatalytic degradation process when the initial concentration of the pollutant is low.

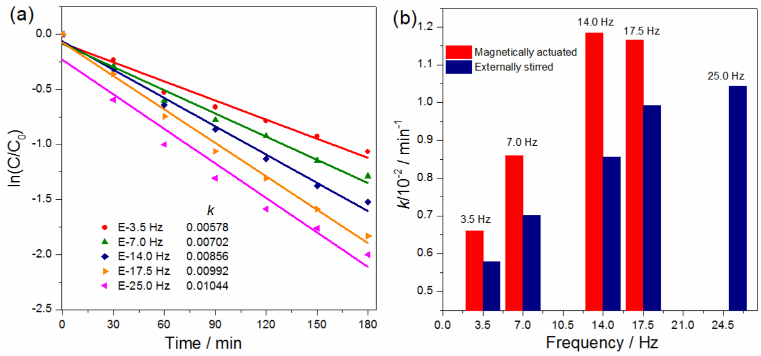

Fig. S16 (a) Photocatalytic kinetics curves of AGT under external stirring with various frequencies. (b) The comparison of reaction rate *k* between externally stirred AGT and magnetically actuated AGT with various frequencies.

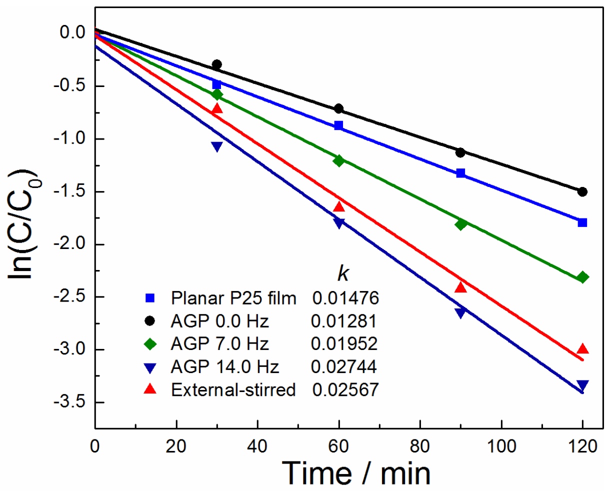

Fig. S17 Photocatalytic kinetics curves of AGP.

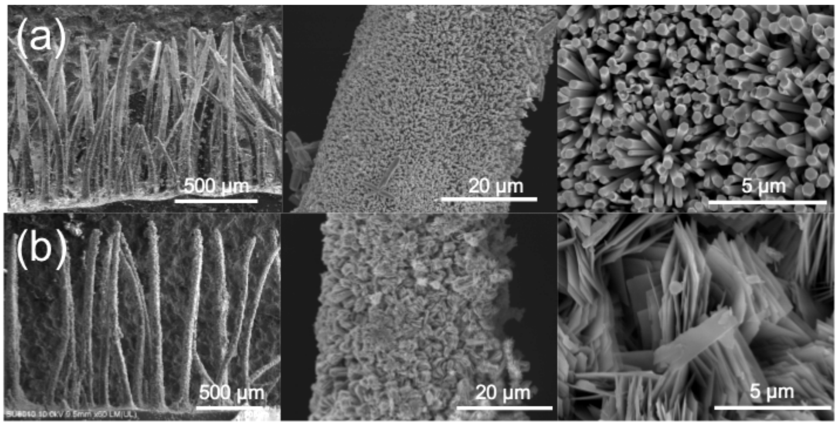

Fig. S18 Efficiency and generality of the new inner-motile photocatalyst film for exploring more ciliary catalysts with different type of catalyst and surface structure. a, FESEM images of ZnO grown on the surface of ciliary array (ciliary array@rG–COOH@ZnO, AGZ). The ciliary arrays were covered by highly dense, radially aligned ZnO nanorods with average diameter of 340 nm. The AGZ could form the ciliary motion induced by magnetic field as like AGT. b, FESEM images of Co_3O_4 grown on the surface of ciliary array (ciliary array@rG–COOH@Co_3O_4, AGC). According to the high magnification FESEM images, high densities of Co_3O_4 nanosheets were vertically grown on the array. These findings provide a further proof of the versatility of the inner-motile photocatalyst film with highly controllable properties, which could be applicable towards designing and assembling other heterogeneous semiconductor (*e.g.* CdS, C_3N_4) and multi-metallic oxides (*e.g.* $BiVO_4$, $NaTaO_3$,).